[3]Steele, B. N., and Harding, M. H., "Applications of Rotating Cylinders for Ship Maneuvering," *Journal of Naval Architecture*, Vol. 5, 1971, pp. 27–29.

[4]Tennant, J. S., Johnson, W. S., and Korthapalli, A., "Rotating Cylinder for Circulation Control on an Airfoil," *Journal of Hydronautics*, Vol. 10, 1976, pp. 102–105.

[5]Tennant, J. S., Johnson, W. S., and Keaton, D. D., "Boundary-Layer Flow from Fixed to Moving Surfaces Including Gap Effects," *Journal of Hydronautics*, Vol. 12, 1978, pp. 81–84.

[6]Mokhtarian, F., and Modi, V. J., "Fluid Dynamics of Airfoils with Moving Surface Boundary-Layer Control," *Journal of Aircraft*, Vol. 25, 1988, pp. 163–169.

[7]Kubo, Y., Modi, V. J., Yasuda, H., and Kato, K., "On the Suppression of Aerodynamic Instability Through the Moving Surface Boundary-Layer Control," *Journal of Wind Engineering and Industrial Aerodynamics*, Vol. 41, 1992, pp. 205–216.

[8]Kubo, Y., Modi, V. J., Kotsubo, C., Nayashida, K., and Kato, K., "Suppression of Wind-Induced Vibrations of Tall Structures Through Moving Surface Boundary-Layer Control," *Journal of Wind Engineering and Industrial Aerodynamics*, Vol. 61, 1995, pp. 181–194.

[9]Modi, V. J., Swinton, P. G., McMillan, K., Lake, P., Mullins, D., and Akutsu, T., "Moving Surface Boundary-Layer Control for Aircraft Operation at High Incidence," *Journal of Aircraft*, Vol. 18, No. 11, 1981, pp. 936–968.

[10]Modi, V. J., Mokhtarian, F., and Yokomizo, T., "Effect of Moving Surfaces on the Airfoil Boundary-Layer Control," *Journal of Aircraft*, Vol. 27, 1990, pp. 42–50.

[11]Modi, V. J., Mokhtarian, F., Fernando, M. S. U. K., and Yokomizo, T., "Moving Surface Boundary-Layer Control as Applied to Two-Dimensional Airfoils," *Journal of Aircraft*, Vol. 28, 1991, pp. 104–112.

[12]Modi, V. J., "Moving Surface Boundary-Layer Control: A Review," *Journal of Fluids and Structures*, Vol. 11, 1997, pp. 627–663.

[13]Ericsson, L. E., "Moving Wall Effect in Relation to Other Dynamic Flow Mechanics," *Journal of Aircraft*, Vol. 31, No. 6, 1994, pp. 1303–1309.

[14]Bhatia, J. C., Durst, F., and Jovanovic, J., "Corrections of Hot-Wire Anemometer Measurements Near Walls," *Journal of Fluid Mechanics*, Vol. 122, 1982, pp. 411–431.

[15]Lee, T., and Budwig, R., "Two Improved Methods for Low-Speed Hot-Wire Calibration," *Measurement Science and Technology*, Vol. 2, 1991, pp. 643–646.

Analytical Approximation for the Mechanics of Airplane Spin

W. F. Phillips* and E. A. Anderson†
Utah State University, Logan, Utah 84322-4130

Nomenclature

$b, \tilde{C}, c, S, \eta$	=	span, section normal force coefficient, chord, planform area, and efficiency factor of surface
I_{xx}, I_{yy}, I_{zz}	=	moments of inertia about the primary axes of roll, pitch, and yaw
ℓ, m, n	=	aerodynamic moments in roll, pitch, and yaw
R, V_d, Ω	=	spin radius, sink rate, and total spin rate
$\boldsymbol{r}, x, y, z$	=	position vector relative to the airplane c.g. and its conventional body-fixed components
T, ω_p	=	propeller thrust and angular velocity
$\boldsymbol{V}, u, v, w$	=	airplane's translational velocity vector and body-fixed components
$\boldsymbol{V}_r, V_N$	=	relative wind and its upward normal or negative z-component
W, X, Y, Z	=	airplane weight and the aerodynamic force components in the x, y, and z directions
ϕ, θ, σ	=	bank angle, elevation angle, and unconventional heading angle relative to the radial plane
$\boldsymbol{\Omega}, p, q, r$	=	airplane's rotational velocity vector and body-fixed components

Subscripts

b, e	=	body-fixed and Earth-oriented components
f, fh, fv	=	fuselage, fuselage horizontal planform, and fuselage vertical planform
h, p, r, v, w	=	horizontal stabilizer, propeller, rudder, vertical stabilizer, and wing

Received 16 May 2002; revision received 25 July 2002; accepted for publication 2 August 2002.

*Professor, Mechanical and Aerospace Engineering Department. Member AIAA.

†Assistant Professor, Mechanical and Aerospace Engineering Department. Senior Member AIAA.

Introduction

AIRPLANE spin was encountered very early in the history of aviation. In the early days of flight, airplane spin was the cause of many fatal accidents. Even today, spin is one of the primary causes of accidents in general aviation.[1,2] The aerodynamic forces and moments produced by the separated flow around a spinning airplane are highly nonlinear and quite complex. Thus, it is very difficult to predict accurately the unsteady motion of a spinning airplane from theoretical analysis alone.[3] Most of what is known about designing airplanes for spin resistance and spin recovery has been obtained from experimental investigation.[4–6] Nevertheless, some insight into the physics of airplane spin can be gained by examining the equations of motion for a fully developed steady spin.

Formulation

Consider the case of steady spin about a vertical axis as shown in Fig. 1. For convenience in writing the equations of motion, an unconventional set of Euler angles will be used. The bank angle and elevation angle are the same as those traditionally used by the aircraft community. As shown in Fig. 1, the heading angle used here, σ, is similar to the conventional azimuth angle, but is measured from the radial plane, not from north. This set of Euler angles describes the orientation of the airplane with respect to an Earth-oriented coordinate system that rotates with the airplane, has the x axis pointed toward the axis of the spin helix, and has the z axis pointed down. The airplane's translational and angular velocity vectors are easily described in this Earth-oriented coordinate system and, thus, can be transformed to conventional body-fixed coordinates using the well-known Euler angle transformation matrix[7]

$$\boldsymbol{V} = \begin{Bmatrix} 0 \\ -R\Omega \\ V_d \end{Bmatrix}_e \equiv \begin{Bmatrix} u \\ v \\ w \end{Bmatrix}_b = \begin{Bmatrix} -V_d \sin\theta - R\Omega \sin\sigma \cos\theta \\ V_d \cos\theta \sin\phi - R\Omega(\cos\sigma \cos\phi + \sin\sigma \sin\theta \sin\phi) \\ V_d \cos\theta \cos\phi + R\Omega(\cos\sigma \sin\phi - \sin\sigma \sin\theta \cos\phi) \end{Bmatrix}_b \tag{1}$$

$$\boldsymbol{\Omega} = \begin{Bmatrix} 0 \\ 0 \\ \Omega \end{Bmatrix}_e \equiv \begin{Bmatrix} p \\ q \\ r \end{Bmatrix}_b = \begin{Bmatrix} -\Omega \sin\theta \\ \Omega \cos\theta \sin\phi \\ \Omega \cos\theta \cos\phi \end{Bmatrix}_b \tag{2}$$

Applying these body-fixed velocity components to Euler's equations of motion[8] and choosing the body-fixed coordinate system to coincide with the primary inertial axes of the airplane gives

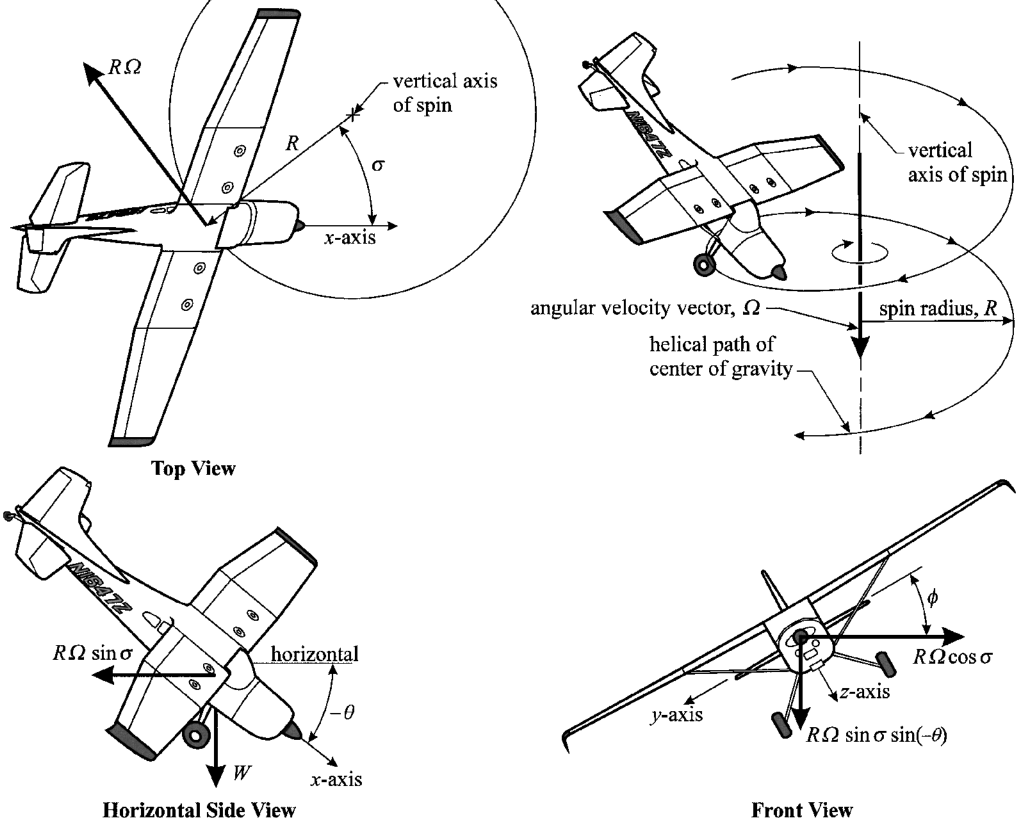

Fig. 1 Top, side, front and isometric views of a spinning airplane.

$$\begin{Bmatrix} T+X \\ Y \\ Z \end{Bmatrix} + W \begin{Bmatrix} -\sin\theta \\ \cos\theta\sin\phi \\ \cos\theta\cos\phi \end{Bmatrix} = \frac{W}{g}\begin{Bmatrix} qw - rv \\ ru - pw \\ pv - qu \end{Bmatrix} = \frac{WR\Omega^2}{g}\begin{Bmatrix} \cos\sigma\cos\theta \\ \cos\sigma\sin\theta\sin\phi - \sin\sigma\cos\phi \\ \cos\sigma\sin\theta\cos\phi + \sin\sigma\sin\phi \end{Bmatrix} \tag{3}$$

$$\begin{Bmatrix} \ell \\ m \\ n \end{Bmatrix} = \begin{Bmatrix} (I_{zz} - I_{yy})qr \\ (I_{xx} - I_{zz})rp \\ (I_{yy} - I_{xx})pq \end{Bmatrix} = \Omega^2 \begin{Bmatrix} (I_{zz} - I_{yy})\cos^2\theta\cos\phi\sin\phi \\ (I_{zz} - I_{xx})\cos\theta\sin\theta\cos\phi \\ (I_{xx} - I_{yy})\cos\theta\sin\theta\sin\phi \end{Bmatrix} \tag{4}$$

The aerodynamic forces and moments depend on the relative wind. The local relative wind at any point on the airplane can be expressed as

$$\boldsymbol{V}_r = -\boldsymbol{V} + \boldsymbol{r}\times\boldsymbol{\Omega} = -\begin{Bmatrix} u \\ v \\ w \end{Bmatrix} + \begin{Bmatrix} yr - zq \\ zp - xr \\ xq - yp \end{Bmatrix} \tag{5}$$

The force acting on a stalled surface is dominated by pressure, which acts normal to the surface. Thus, the total force on the wing and horizontal stabilizer is closely aligned with the negative z direction and is proportional to the square of the normal velocity, which is the negative z component of relative wind,

$$V_N^2 = w^2 + 2ypw + y^2p^2 - 2xqw - 2xypq + x^2q^2 \tag{6}$$

For example, the force and associated moments produced on the wing are then given by

$$\begin{Bmatrix} Z_w \\ \ell_w \\ m_w \end{Bmatrix} = \frac{1}{2}\rho\tilde{C}_w \int_{-b_w/2}^{b_w/2} \begin{Bmatrix} -V_N^2 \\ -yV_N^2 \\ xV_N^2 \end{Bmatrix} c_w\,\mathrm{d}y = \frac{1}{2}\rho S_w\tilde{C}_w \begin{Bmatrix} -w^2 - \overline{y_w^2}p^2 + 2\overline{x_w}qw - \overline{x_w^2}q^2 \\ -2\overline{y_w^2}pw + 2\overline{x_w y_w^2}pq \\ \overline{x_w}w^2 + \overline{x_w y_w^2}p^2 - 2\overline{x_w^2}qw + \overline{x_w^3}q^2 \end{Bmatrix} \tag{7}$$

where

$$\overline{f_w^k} \equiv \frac{1}{S_w}\int_{-b_w/2}^{b_w/2} f^k c_w\,\mathrm{d}y$$

Similar results can be obtained for the other surfaces of the airplane, with the side force and yawing moment being proportional to the square of the sideslip velocity.

A rotating propeller produces a yawing moment that is proportional to the normal component of relative wind. Because an airplane's normal velocity component is typically quite large in a spin, a rotating propeller can contribute significantly to the yawing moment needed to initiate and sustain the spin. If the propeller's rotational velocity is sufficiently large compared to the relative wind, the propeller yawing moment can be approximated as[9]

$$n_p = \frac{\partial n_p}{\partial V_N}V_N \cong -\frac{TV_N}{\omega_p} = \frac{\partial n_p}{\partial V_N}(w + y_p p - x_p q) \cong -\frac{T}{\omega_p}(w + y_p p - x_p q) \tag{8}$$

where the propeller's angular velocity is positive for a right-hand propeller and negative for a left-hand propeller. Notice that even the counter-rotating propellers of a multiengine airplane will produce a net yawing moment in a spin. For counter-rotating propellers mounted equal distance on opposite sides of the c.g., the contributions from the first and third terms in Eq. (8) will cancel because ω_p will be positive for one propeller and negative for the other. However, the contributions from the second term in Eq. (8) will add, because both ω_p and y_p have opposite signs.

The force and moment components for the complete airplane can be approximated by summing contributions from all surfaces. For each surface, the contributions are evaluated from integrals similar to those used to evaluate the wing contribution in Eq. (7). When Eq. (5) is used for the relative wind, the thrust is assumed to be a linear function of forward velocity, and contributions from the wing, horizontal stabilizer, vertical stabilizer, fuselage, propellers, and rudder are combined, the net force and moment components for the complete airplane are approximated as

$$\begin{Bmatrix} T+X \\ Y \\ Z \end{Bmatrix} = \frac{\rho S_w}{2}\begin{Bmatrix} V_{T0}^2 + V_{T1}u + C_X u^2 \\ \left(C_{Y1}v^2 + 2C_{n1}b_w rv + C_{Y2}b_w^2 r^2 - 2C_{Y3}b_w pv \right. \\ \left. - 2C_{n3}b_w^2 pr + C_{Y4}b_w^2 p^2\right)\Omega/|\Omega| \\ -C_{N1}w^2 - C_{N2}b_w^2 p^2 + 2C_{m1}b_w qw - C_{N3}b_w^2 q^2 \end{Bmatrix} \tag{9}$$

$$\begin{Bmatrix} \ell \\ m \\ n \end{Bmatrix} = \frac{\rho S_w b_w}{2}\begin{Bmatrix} -2C_{N2}b_w pw + 2C_{m2}b_w^2 pq \\ C_{m1}w^2 + C_{m2}b_w^2 p^2 - 2C_{N3}b_w qw + C_{m3}b_w^2 q^2 \\ \left[\left(C_{n1}v^2 + 2C_{Y2}b_w rv + C_{n2}b_w^2 r^2 - 2C_{n3}b_w pv \right.\right. \\ \left. - 2C_{n4}b_w^2 pr + C_{n5}b_w^2 p^2\right)\Omega/|\Omega| - V_{p1}w \\ \left. - V_{p2}b_w p + V_{p3}b_w q + (\Delta C_n)_r u^2\right] \end{Bmatrix} \tag{10}$$

where

$$V_{T0}^2 \equiv \frac{2T_{u=0}}{\rho S_w}, \qquad V_{T1} \equiv \frac{2}{\rho S_w}\frac{\partial T}{\partial u}, \qquad C_X \equiv \frac{X}{\frac{1}{2}\rho S_w u^2}$$

$$(\Delta C_n)_r \equiv \frac{(\Delta n)_r}{\frac{1}{2}\rho S_w b_w u^2}, \qquad C_{N1} \equiv \frac{S_w\tilde{C}_w + S_h\tilde{C}_h + S_{fh}\tilde{C}_f}{S_w}$$

$$C_{N2} \equiv \frac{S_w\tilde{C}_w\overline{y_w^2} + S_h\tilde{C}_h\overline{y_h^2} + S_{fh}\tilde{C}_f\overline{y_{fh}^2}}{S_w b_w^2}$$

$$C_{N3} \equiv \frac{S_w\tilde{C}_w\overline{x_w^2} + S_h\tilde{C}_h\overline{x_h^2} + S_{fh}\tilde{C}_f\overline{x_{fh}^2}}{S_w b_w^2}$$

$$C_{Y1} \equiv \frac{\eta_v S_v\tilde{C}_v + S_{fv}\tilde{C}_f}{S_w}, \qquad C_{Y2} \equiv \frac{\eta_v S_v\tilde{C}_v\overline{x_v^2} + S_{fv}\tilde{C}_f\overline{x_{fv}^2}}{S_w b_w^2}$$

$$C_{Y3} \equiv \frac{\eta_v S_v\tilde{C}_v\overline{z_v} + S_{fv}\tilde{C}_f\overline{z_{fv}}}{S_w b_w}, \qquad C_{Y4} \equiv \frac{\eta_v S_v\tilde{C}_v\overline{z_v^2} + S_{fv}\tilde{C}_f\overline{z_{fv}^2}}{S_w b_w^2}$$

$$C_{m1} \equiv \frac{S_w\tilde{C}_w\overline{x_w} + S_h\tilde{C}_h\overline{x_h} + S_{fh}\tilde{C}_f\overline{x_{fh}}}{S_w b_w}$$

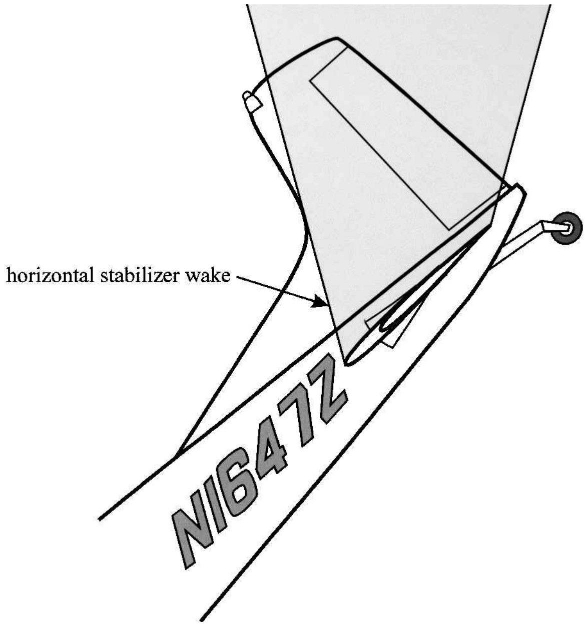

Fig. 2 Schematic diagram showing the reduction in yaw stability due to the vertical stabilizer being partially shadowed by the wake of the horizontal stabilizer.

$$C_{m2} \equiv \frac{S_w\tilde{C}_w\overline{x_w y_w^2} + S_h\tilde{C}_h\overline{x_h y_h^2} + S_{fh}\tilde{C}_f\overline{x_{fh}y_{fh}^2}}{S_w b_w^3}$$

$$C_{m3} \equiv \frac{S_w\tilde{C}_w\overline{x_w^3} + S_h\tilde{C}_h\overline{x_h^3} + S_{fh}\tilde{C}_f\overline{x_{fh}^3}}{S_w b_w^3}$$

$$C_{n1} \equiv \frac{\eta_v S_v\tilde{C}_v\overline{x_v} + S_{fv}\tilde{C}_f\overline{x_{fv}}}{S_w b_w}, \qquad C_{n2} \equiv \frac{\eta_v S_v\tilde{C}_v\overline{x_v^3} + S_{fv}\tilde{C}_f\overline{x_{fv}^3}}{S_w b_w^3}$$

$$C_{n3} \equiv \frac{\eta_v S_v\tilde{C}_v\overline{x_v z_v} + S_{fv}\tilde{C}_f\overline{x_{fv}z_{fv}}}{S_w b_w^2}$$

$$C_{n4} \equiv \frac{\eta_v S_v\tilde{C}_v\overline{x_v^2 z_v} + S_{fv}\tilde{C}_f\overline{x_{fv}^2 z_{fv}}}{S_w b_w^3}$$

$$C_{n5} \equiv \frac{\eta_v S_v\tilde{C}_v\overline{x_v z_v^2} + S_{fv}\tilde{C}_f\overline{x_{fv}z_{fv}^2}}{S_w b_w^3}$$

$$V_{p1} = -\sum \frac{2}{\rho S_w b_w}\frac{\partial n_p}{\partial V_N}, \qquad V_{p2} = -\sum \frac{2y_p}{\rho S_w b_w^2}\frac{\partial n_p}{\partial V_N}$$

$$V_{p3} = -\sum \frac{2x_p}{\rho S_w b_w^2}\frac{\partial n_p}{\partial V_N}$$

The vertical stabilizer efficiency factor is less than unity to account for the reduced yaw stability resulting from the vertical stabilizer being partly shadowed by the wake of the horizontal stabilizer as shown in Fig. 2. This efficiency factor can be approximated as the ratio of the unshadowed stabilizer area to the total stabilizer area. Using Eqs. (1), (2), (9), and (10) in Eqs. (3) and (4) yields a system of six nonlinear equations, which can be solved numerically for the six unknowns, R, V_d, Ω, ϕ, θ, and σ.

Approximate Closed-Form Solution

Although numerical solution of the nonlinear spin formulation presented here is rather straightforward, it does not provide the insight into the physics of airplane spin that could be afforded by a simple closed-form solution. Therefore, some further assumptions will now be applied to this formulation with the goal of obtaining an approximate closed-form solution.

The difference between the thrust and the axial component of drag is typically quite small compared to the normal force developed on a stalled wing. Furthermore, it is often assumed that both ϕ and σ are small in a spin.[1,2] If it is also assumed that the wing and tail are in close vertical alignment with the c.g., $z \cong 0$, a reasonable first approximation for the aerodynamic forces and moments can be obtained by using

$$V_{T0}^2 + V_{T1}u + C_X u^2 \cong C_{Y3} \cong C_{Y4} \cong C_{n3} \cong C_{n4} \cong C_{n5} \cong 0$$

$$\begin{Bmatrix} u \\ v \\ w \end{Bmatrix} \cong \begin{Bmatrix} -V_d \sin\theta \\ -R\Omega \\ V_d \cos\theta \end{Bmatrix}, \qquad \begin{Bmatrix} p \\ q \\ r \end{Bmatrix} \cong \begin{Bmatrix} -\Omega \sin\theta \\ 0 \\ \Omega \cos\theta \end{Bmatrix}$$

When these approximations are applied and the small angle approximation for ϕ and σ are used on the right-hand sides of Eqs. (3) and (4), the formulation can be simplified and rearranged to eliminate ϕ and σ. Thus, the formulation is reduced to a system of four nonlinear equations that can be directly solved for Ω, R, V_d, and $(\Delta C_n)_r$, all as a function of θ,

$$\Omega^2 = \frac{2W}{\rho S_w C_{N1} \cos\theta \sin^2\theta} \times \left[\frac{2(I_{zz} - I_{xx})}{\rho S_w b_w C_{m1} \tan\theta} - \frac{C_{m2} b_w^2}{C_{m1}} + \frac{C_{N2} b_w^2}{C_{N1}} \right]^{-1} \tag{11}$$

$$R = -\frac{g \tan\theta}{\Omega^2} \tag{12}$$

$$V_d^2 = \frac{2W}{\rho S_w C_{N1} \cos^3\theta} - \frac{C_{N2} b_w^2 \Omega^2 \tan^2\theta}{C_{N1}} \tag{13}$$

$$(\Delta C_n)_r = \frac{2C_{N2}(I_{xx} - I_{yy}) b_w \Omega}{(I_{zz} - I_{yy}) V_d} + \frac{V_{p1} \cos\theta}{V_d \sin^2\theta} - \frac{V_{p2} b_w \Omega}{V_d^2 \sin\theta} - \left(\frac{C_{n1} R^2}{\sin^2\theta} - \frac{2C_{Y2} b_w R}{\sin\theta \tan\theta} + \frac{C_{n2} b_w^2}{\tan^2\theta} \right) \frac{\Omega|\Omega|}{V_d^2} \tag{14}$$

Typically, the elevation angle required to support a fully developed steady spin is not known a priori. Instead, the yaw control coefficient might be known for a given rudder deflection. For example, $(\Delta C_n)_r$ is zero with no rudder deflection. When Eqs. (11–13) are used to eliminate Ω, R, and V_d, Eq. (14) provides a single nonlinear equation for the unknown elevation angle. The roots of this equation, if they exist, are the elevation angles that will support a fully developed steady spin, with the assumption that both ϕ and σ are small.

Figure 3 shows examples of spin characteristics, which were predicted from Eqs. (11–14) for light aircraft, using $\tilde{C}_f = 1.0$ and $\tilde{C}_w = \tilde{C}_h = \tilde{C}_v = 2.0$. (Thin airfoil sections are assumed.) Notice that the spin radius predicted for a flat spin is much smaller than that for a steep spin. The more common steep spins, which typically occur with the airplane's nose about 40–60 deg below horizontal, have predicted spin radii of about 25–30% of the wingspan. Also notice that the predicted sink rate is much larger for a steep spin than for a flat spin. For the common elevation angle range between −40 and −60 deg, the current analytical model predicts sink rates ranging from about 100 to 200 ft/s (30–60m/s), which is in good agreement with experimental data.[4] For this same range of elevation angles, the predicted spin rate only varies from approximately 110 to 140 deg/s. This also agrees with experimental observation.

For the airplane used to generate Fig. 3a (with $\eta_v = 0.1$), this approximate analytical model predicts that there are two elevation angles that will support a steady spin with no rudder deflection. These correspond to a flat spin at about −12 deg and a steep spin at about −58 deg. The flat spin would most likely be difficult to initiate because the airplane's nose usually drops very rapidly when the wing stalls. The spin characteristics predicted from Eqs. (11–14) for a more typical modern general aviation airplane are shown in Fig. 3b (using $\eta_v = 0.5$). For this airplane, the model predicts that yaw control input is required to maintain any spin, except in the limit

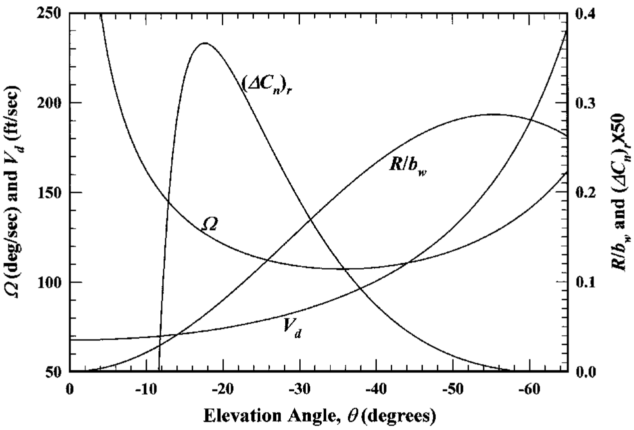

a) Design with prospin characteristics

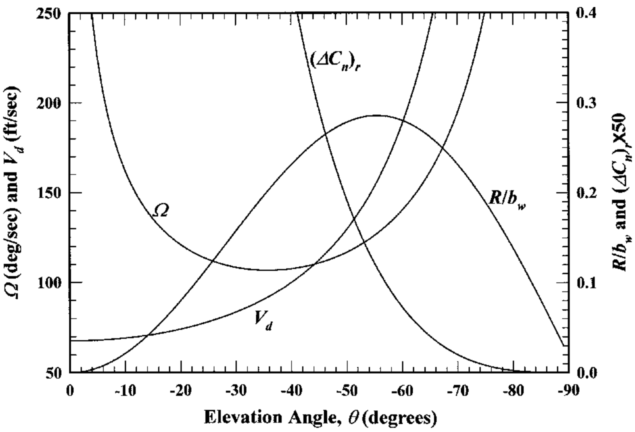

b) Spin-resistant design

Fig. 3 Examples of predicted spin characteristics for light airplanes.

as the elevation angle approaches −90 deg. Such a steep maneuver is not a spin at all but a spiral dive. The present analytical model does not apply in this case because the angle of attack would be below stall. For elevation angles steeper than about −65 or −70 deg, the present model predicts very high sink and spin rates. These results are not realistic because the predicted airspeeds are beyond those for which compressibility becomes significant, and the model does not account for compressibility.

Conclusions

Note that the closed-form analytical solution presented here is based on an approximation to the steady equations of motion for airplane spin. In reality, the net axial force will not be exactly zero in a spin. However, compared to the normal force generated on the stalled wing, this force is small. Furthermore, the angles ϕ and σ are not necessarily small in a spin. Thus, the model does not apply to all spins and all airplanes. The model is based on the assumption of large angle of attack and, thus, does not apply to extremely steep spins and spiral dives because the angle of attack becomes small in such cases. Moreover, the present model does not account for compressibility effects, which become important in very steep spins and dives. Nevertheless, this approximate model can provide some valuable insight into the physics of airplane spin.

References

[1] McCormick, B. W., "Spinning," *Aerodynamics, Aeronautics, and Flight Mechanics*, 2nd ed., Wiley, New York, 1995, pp. 577–582.

[2] Pamadi, B. N., "Airplane Spin," *Performance, Stability, Dynamics, and Control of Airplanes*, AIAA, Reston, VA, 1998, pp. 646–670.

[3] Anglin, E. L., "Analytical Study of Effects of Product of Inertia on Airplane Spin Entries, Developed Spins, and Spin Recoveries," NASA TN-D-2754, April 1965.

[4] Stough, H. P., DiCarlo, D. J., and Patton, J. M., "Flight Investigation of Stall, Spin, and Recovery Characteristics of a Low-Wing, Single-Engine, T-Tail Light Airplane," NASA TR-2427, May 1985.

[5]Fremaux, C. M., "Spin-Tunnel Investigation of a 1/28-Scale Model of the NASA F-18 High Alpha Research Vehicle (HARV) With and Without Tails," NASA TR-201687, April 1997.

[6]Croom, M., Kenney, H., Murri, D., and Lawson, K., "Research on the F/A-18E/F Using a 22%-Dynamically Scaled Drop Model," AIAA Paper 2000-3913, Aug. 2000.

[7]Phillips, W. F., Hailey, C. E., and Gebert, G. A., "Review of Attitude Representations Used for Aircraft Kinematics," *Journal of Aircraft*, Vol. 38, No. 4, 2001, pp. 718–737.

[8]Etkin, B., and Reid, L. D., "Euler's Equations of Motion," *Dynamics of Flight: Stability and Control*, 3rd ed., Wiley, New York, 1996, pp. 100–101.

[9]Phillips, W. F., and Anderson, E. A., "Predicting the Contribution of Running Propellers to Aircraft Stability Derivatives," AIAA Paper 2002-0390, Jan. 2002.

Estimating the Low-Speed Sidewash Gradient on a Vertical Stabilizer

W. F. Phillips*
Utah State University, Logan, Utah 84322-4130

Nomenclature

b = wingspan
b' = wingtip vortex spacing
C_{Lw} = wing lift coefficient
R_{Aw} = wing aspect ratio
V_z = z component of induced velocity
V_∞ = magnitude of the freestream velocity
x = axial coordinate
$\bar{x}$ = dimensionless axial coordinate, $2x/b$
y = normal coordinate
$\bar{y}$ = dimensionless normal coordinate, $2y/b$
z = spanwise coordinate, measured from the aircraft plane of symmetry
$\bar{z}$ = dimensionless spanwise coordinate, $2z/b$
z' = spanwise coordinate, measured from the centerline midway between the two wingtip vortices
$\bar{z}'$ = dimensionless spanwise coordinate, $2z'/b$
β = sideslip angle
Γ_{wt} = wingtip vortex strength
ε_s = sidewash angle
κ_b = spacing between the wingtip vortices divided by the wingspan
κ_v = ratio of wingtip vortex strength to that of an elliptic wing having the same lift coefficient and aspect ratio
κ_β = sidewash factor
Λ = quarter-chord wing sweep angle

Introduction

THE sidewash induced on a vertical stabilizer by the wingtip vortices shed from the main wing can have a significant effect on the static yaw stability of an airplane. For a vertical stabilizer mounted above the main wing, the sidewash gradient is negative and has a stabilizing effect on the airplane. The sidewash gradient produced by the wingtip vortices can be estimated using a vortex model that was recently presented for predicting the downwash produced by a wing of arbitrary planform.[1] This vortex model, which is shown in Fig. 1, was originally proposed by McCormick[2] for estimating the downwash produced by an elliptic wing.

Analytical Model

Relative to the coordinate system shown in Fig. 1, the z component of velocity induced by this model of the wingtip vortices, at the arbitrary point in space (x, y, z), is readily found from the Biot–Savart law to be

$$V_z = \frac{\Gamma_{\mathrm{wt}}}{4\pi}\left\{\frac{y}{y^2 + \left(z + \frac{1}{2}b'\right)^2}\left[1 + \frac{x - \frac{1}{2}b'\tan\Lambda}{\sqrt{\left(x - \frac{1}{2}b'\tan\Lambda\right)^2 + y^2 + \left(z + \frac{1}{2}b'\right)^2}}\right] - \frac{y}{y^2 + \left(z - \frac{1}{2}b'\right)^2}\left[1 + \frac{x - \frac{1}{2}b'\tan\Lambda}{\sqrt{\left(x - \frac{1}{2}b'\tan\Lambda\right)^2 + y^2 + \left(z - \frac{1}{2}b'\right)^2}}\right]\right\} \tag{1}$$

The wingtip vortex strength is proportional to the product of the wing lift coefficient and airspeed. The wingtip vortex strength and spacing can be evaluated from lifting-line theory.[1] When the traditional sign convention that sidewash is positive from left to right is used, Eq. (1) is combined with lifting-line theory, and the small angle approximation is applied, the sidewash angle can be written as

$$\varepsilon_s = -\frac{V_z}{V_\infty} = \frac{C_{Lw}\kappa_v}{\pi^2 R_{Aw}}\left\{\frac{\bar{y}}{\bar{y}^2 + (\bar{z} - \kappa_b)^2}\left[1 + \frac{\bar{x} - \kappa_b\tan\Lambda}{\sqrt{(\bar{x} - \kappa_b\tan\Lambda)^2 + \bar{y}^2 + (\bar{z} - \kappa_b)^2}}\right] - \frac{\bar{y}}{\bar{y}^2 + (\bar{z} + \kappa_b)^2}\left[1 + \frac{\bar{x} - \kappa_b\tan\Lambda}{\sqrt{(\bar{x} - \kappa_b\tan\Lambda)^2 + \bar{y}^2 + (\bar{z} + \kappa_b)^2}}\right]\right\} \tag{2}$$

where the parameters κ_v and κ_b can be evaluated analytically from the known planform shape of the wing using the results presented by Phillips et al.[1]

Equation (2) can be directly applied to determine the sidewash angle only when the sideslip angle is zero and the aircraft plane of

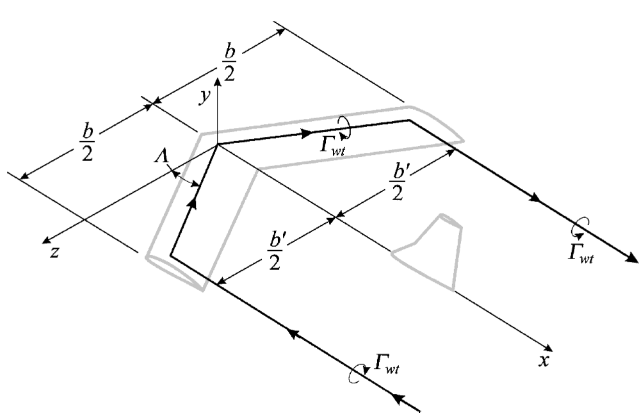

Fig. 1 Vortex model used to estimate the sidewash gradient for the vertical stabilizer.

Received 30 May 2002; revision received 2 August 2002; accepted for publication 8 August 2002.

*Professor, Mechanical and Aerospace Engineering Department. Member AIAA.